Contributions of Indian Ocean and Monsoon Biases to the Excessive Biennial ENSO in CCSM3

Jin-Yi Yu[1], Fengpeng Sun, and Hsun-Ying Kao

Department of Earth System Science
University of California-Irvine

Revised on October 13, 2008

Submitted to Journal of Climate

[1] Corresponding Author: Dr. Jin-Yi Yu, Department of Earth System Science, University of California, Irvine, CA 92697-3100. E-mail: jyyu@uci.edu.

ABSTRACT

The Community Climate System Model 3.0 (CCSM3) is known to produce many aspects of El Niño-Southern Oscillation (ENSO) realistically, but the simulated ENSO exhibits an overly strong biennial periodicity. Hypotheses on the cause of this excessive biennial tendency have thus far focused primarily on the model's biases within the tropical Pacific. This study conducts CCSM3 experiments to show that the model's biases in simulating the Indian Ocean mean sea surface temperatures (SSTs) and the Indian and Australian monsoon variability also contribute to the biennial ENSO tendency. Two CCSM3 simulations are contrasted: a control run that includes global ocean-atmosphere coupling and an experiment in which the air-sea coupling in the tropical Indian Ocean is turned off by replacing simulated SSTs with an observed monthly climatology. The decoupling experiment removes CCSM3's warm bias in the tropical Indian Ocean and reduces the biennial variability in Indian and Australian monsoons by about 40% and 60%, respectively. The excessive biennial ENSO is found to reduce dramatically by about 75% in the decoupled experiment. It is shown that the biennial monsoon variability in CCSM3 excites an anomalous surface wind pattern in the western Pacific that projects well into the wind pattern associated with the onset phase of the simulated biennial ENSO. Therefore, the biennial monsoon variability is very effective in exciting biennial ENSO variability CCSM3. The warm SST bias in the tropical Indian Ocean also increases ENSO variability by inducing stronger mean surface easterlies along the equatorial Pacific, which strengthen the Pacific ocean-atmosphere coupling and enhance the ENSO intensity.

1. Introduction

The Community Climate System Model 3.0 (CCSM3) (Collins et al. 2006) of National Center for Atmospheric Research (NCAR) is able to realistically replicate many observed characteristics of El Niño-Southern Oscillation (ENSO), but the simulated ENSO is known to exhibit an overly strong biennial (~2 years) periodicity (Deser et al. 2006). The causes of this excessive biennial tendency have not yet been fully determined. Since the fundamental dynamics of ENSO resides within the tropical Pacific Ocean, hypotheses on the causes of this biennial tendency have thus far focused primarily on the model's biases inside the Pacific basin. One well-accepted explanation is that the meridional scale of the atmospheric response to ENSO's sea surface temperature (SST) anomalies is too narrowly confined to the equator and therefore fastens the turnabout of the ENSO cycle (Deser et al. 2006). Based on the charge-recharge oscillator theory of ENSO (Wyrtki 1975; Jin 1997), the strength and meridional scale of the surface wind response set the meridional scale of the warm water volume involved in the recharge/discharge process and may affect the ENSO frequency.

Nevertheless, interannual climate variability originated from the Indian Ocean and the Indian and Australian monsoons could possibly interplay with the ENSO dynamics. The potential physical processes that allow the Indian Ocean and monsoons to influence the ENSO properties have been suggested in several recent studies (e.g., Yu et al. 2002; Wu and Kirtman 2004; Terray and Dominiak 2005; Kug and Kang 2006; Kug et al. 2006). Among them, Wu and Kirtman (2004) demonstrated that SST variations in the Indian Ocean provide a positive feedback to ENSO

intensity by affecting surface winds in the western Pacific. Terray and Dominiak (2005) argued that the southeastern Indian Ocean SST anomalies act as persistent remote forcing to trigger anomalous surface winds in the western equatorial Pacific and regional Hadley circulation in the south Pacific, both of which further affect the evolution of ENSO. Kug and Kang (2006) suggested that the basin-scale warming/cooling in the Indian Ocean, a typical Indian Ocean response to ENSO, can produce surface wind anomalies in the western Pacific that enhance eastward-propagating oceanic Kevin waves to accelerate the turnabout of ENSO, and therefore shorten the period of ENSO cycle. In their argument, the interaction between ENSO and Indian Ocean might generate a biennial tendency for ENSO.

Additionally, it is known that both the Indian and Australian monsoons have a strong biennial variability, which is part of the so-called Tropospheric Biennial Oscillation (TBO) (Meehl 1987, 1993; Li et al. 2006). This is a tendency for the Indian and Australian monsoons to flip-flop back and forth between strong and weak monsoon years. Years with strong summer monsoon rainfall tend to be followed by ones with weak rainfall and vice versa (e.g., Mooley and Parthasarathy 1984; Meehl 1987, 1993). The TBO was suggested to have its own dynamics, independent of ENSO (e.g., Meehl 1987, 1993) and possibly force the biennial component of ENSO. Most TBO theories suggest air-sea interactions over the tropical Indo-Pacific sector responsible for the biennial variability in the Indian-Australian monsoons (e.g., Meehl 1987, 1993; Chang and Li 2000; Webster et al. 2001; Li et al. 2006). For example, Webster et al. (2001) suggested that the observed variability in the Indian and Australian monsoons is self-regulated by the negative feedbacks between the atmosphere and the Indian Ocean involving the wind-driven

Ekman transport. Furthermore, the biennial variability associated with the TBO in the ENSO-monsoon system has been documented in coupled atmosphere-ocean general circulation models (CGCMs) (e.q., Ogasawara et al. 1999; Loschnigg et al. 2003) and has been shown to have a significant component arising from the Indian Ocean (Loschnigg et al. 2003).

In this study, we turn off the ocean-atmosphere coupling in the Indian Ocean in one CCSM3 experiment, which is expected to reduce the biennial monsoon variability. We then compare this experiment with the CCSM3 control simulation to examine the contributions of the Indian Ocean and Indian-Australian monsoons to the biennial ENSO tendency in the model. Such basin-coupling/decoupling experiments had been performed to study the inter-basin interactions between the Indian and Pacific Oceans with other CGCMs (e.g., Yu et al. 2002; Wu and Kirtman 2004; Kug et al. 2006) but not yet with CCSM3. In the decoupled experiment, the Indian Ocean decoupling is made possible by replacing the simulated SSTs in the basin with a monthly SST climatology from observations. By doing so, the SST bias in the tropical Indian Ocean is also removed from CCSM3. By contrasting the decoupled experiment to the control run, we show in this study that both the overly strong biennial monsoon variability and the Indian Ocean SST bias contribute to the excessive biennial ENSO tendency in CCSM3. Possible mechanisms are proposed to explain how the linkages are established.

2. Model and Experiments

The control run used in this study is the "1990 Control Run" produced by NCAR with a

T42_gx1v3 configuration of CCSM3, in which model parameters are set to present-day values including a global-mean annually averaged mixed ratio of 355 ppmv for the CO_2 concentration and the Year 1990 values for the default solar constant and trace gas concentrations (see Collins et al. 2006). In this control run, the atmosphere is coupled to global oceans. Monthly outputs of the "1990 Control Run" were downloaded from the Earth System Grid project (http://www.earthsystemgrid.org/). In the decoupled experiment, the SSTs simulated by the ocean component of CCSM3 in the tropical Indian Ocean (between 30°S and 30°N) are replaced with the observed monthly SST climatology (1957-1996) from the Hadley Centre Sea Ice and Sea Surface Temperature data set (HadISST) (Rayner et al. 2003). The SST replacement makes the Indian Ocean-decoupled experiment different from the control run in two aspects. The first is that the Indian Ocean SST variability is removed. The second is that the mean SST bias in the Indian Ocean is also removed. Other model configurations are the same as those in the control run. To reduce the computation time needed to spin up the decoupled experiment, its integration was restarted from the January condition of model year 940 of the "1990 Control Run". The last 50 years of its 70-year integration are analyzed. Simulations of years 950-999 from the control run are analyzed for comparisons with the decoupled experiment. All the anomalies are calculated as the deviations from the long-term mean of the seasonal cycle.

3. Results

Figures 1a and 1b show, respectively, the long-term mean SSTs from the observation (HadISST) and the control run. The general pattern of the observed SST distribution is

reasonably captured in the control run. The simulated warm pool covers both the western Pacific Ocean and the Indian Ocean. A cold tongue is produced in the eastern equatorial Pacific. Model deficiencies also exist. Compared to the observations, the control run produces a too-warm warm pool in the tropical Indian Ocean. The 29°C isotherm in the control run covers the tropical Indian Ocean, while by contrast the 29°C isotherm in the observation does not show up in the Indian Ocean but is confined to the western Pacific. The simulated cold tongue in the eastern Pacific tends to be too cold and too westward extended compared to the observations, which is a well-known bias of CCSM3 (Deser et al. 2006). Figure 1c shows the mean SST difference between the two CCSM3 simulations, with the decoupled experiment mean SSTs subtracted by those of the control run. Since the tropical Indian Ocean SSTs in the decoupled experiment are prescribed from the observations, the Indian Ocean SST difference shown in Figure 1c represents the opposite of the SST bias of the control run. The negative difference in Figure 1c indicates that the control run produces a warm bias in the tropical Indian Ocean between 10°S and 10°N and near Sumatra. In the equatorial eastern-to-central Pacific, the decoupled experiment produces warmer SSTs than the control run, indicating that the cold bias of the cold tongue is reduced in the decoupled experiment. We also find that the mean surface easterly along the equatorial Pacific is weaker in the decoupled experiment than in the control run (not shown). These differences suggest that, in the decoupled experiment, the colder mean SST in the tropical Indian Ocean induces a weaker mean easterly in the Pacific, which may then reduce the westward advection of the cold tongue and result in a warmer equatorial Pacific than in the control run.

We then examine the impact of the Indian Ocean decoupling on the ENSO variability.

Figure 2 shows the standard deviations of the interannual SST anomalies calculated from the control run and the decoupled experiment. The maximum standard deviation produced by the control run (Figure 2a) is close to the observations, which is about 1.2°C. However, the simulated ENSO structure locates too far away from the coast compared to the observed. This is a known deficiency of CCSM3 in ENSO simulation (Deser et al. 2006). Figure 2b shows that the ENSO SST variability in the decoupled experiment is significantly reduced. The reduction of the standard deviation is as large as 0.3°C in the central equatorial Pacific. This result is consistent with previous studies of Yu et al. (2002) using the UCLA CGCM and Wu and Kirtman (200) using the COLA CGCM. They both found the Indian Ocean coupling could increase ENSO intensity in CGCMs. It should be noted that the spatial pattern of the ENSO SST anomalies is not changed by the Indian Ocean coupling. The SST anomalies still centered more toward the central Pacific. We also notice little change in the phase locking property of ENSO between the control and the decoupled simulations. Figure 3 shows the seasonal variations of the standard deviation of the Niño3.4 (5°S-5°N, 170°W-120°W) SST anomalies calculated from the two CCSM3 simulations. Although the month of the minimum standard deviation shifts from March in the control run to June in the decoupled experiment, the general features in the phase locking remain unchanged. In particular, the mature phase of the simulated ENSO occurs in boreal winter in both simulations.

We further examine in Figure 4 the power spectra of monthly Niño3.4 SST anomalies calculated from the two simulations. As expected, a near 2-year single peak dominates the power spectrum of the control run (blue). This excessively strong biennial ENSO signal is reduced

dramatically by about 75% in the decoupled experiment (red). It is important to note that the Indian Ocean decoupling does not increase the power of ENSO in other frequency bands. According to the feedback mechanism proposed by Kug and Kang (2006), by turning off the ocean-atmosphere coupling in the Indian Ocean and its feedback to ENSO, the turnabout of ENSO cycles could be lengthened and ENSO's recurrence may shift to lower frequencies. But no such a frequency shift is found in our CCSM3 simulations. One possible explanation for this difference is that the way the model ENSO interacts with the Indian Ocean in CCSM3 is not exactly the same as in the observation.

Two monsoon rainfall indices were used to examine the changes of monsoon variability between the two CCSM3 simulations. The Indian monsoon rainfall index (IMRI) is adopted from Yu et al. (2003), which is defined as the monthly rainfall anomalies averaged over the area between 65°E and 100°E and between 10°N and 30°N. The Australian monsoon rainfall index (AMRI) is defined following Hung and Yanai (2004), which is the monthly rainfall anomalies averaged over the area between 110E°and 150°E and between 2°S and 15°S. Figure 5 shows the power spectra calculated from the simulations and the 28-year (1979-2006) Global Precipitation Climatology Project (GPCP) Version 2 monthly dataset (Adler et al. 2003). In the observation (black), both the IMRI and AMRI show a statistically significant (at the 95% level) spectral peak near the 2-year band. The observed AMRI has another major and larger spectral peak at the 4~5-year band. In the control run (blue), a biennial spectral peak dominates both monsoon indices. The observed large 4~5-year peak for the AMRI does not occur in the control run. This is likely due to the lack of a 4-5year component of ENSO in CCSM3. And particularly, the

simulated biennial Indian monsoon variability is 25% stronger than the observed. In the decoupled experiment (red), the biennial monsoon variability is significantly reduced from the control run for the both monsoon indices. The reduction is about 60% for the Australian monsoon and 40% for the Indian monsoon. Figure 5 suggests that the Indian Ocean coupling is important to the biennial variability of the Indian and Australian monsoons, which is consistent with the existing TBO theories that emphasize air-sea interactions in the Indian Ocean for biennial variability.

The coherent decreases in the biennial monsoon variability and the biennial ENSO intensity caused by the Indian Ocean decoupling suggest that the excessive biennial ENSO in CCSM3 might be related to the biennial monsoon variability in the model. When the Indian Ocean decoupling reduces the biennial monsoon variability, the biennial ENSO variability is reduced accordingly. To make sense of this mechanism, it is necessary to explain how the Indian and Australian monsoon variability in CCSM3 can so effectively excite the ENSO activity. One possibility is that the surface wind stress anomalies associated with the monsoon variations match the anomalous wind pattern needed for the onset of biennial ENSO events. Since the biennial ENSO in the control run matures in boreal winter due to its phase locking to the seasonal cycle (see Figure 3), its onset time should occur in the preceding summer, about 5-6 months ahead of the mature phase.

By considering that, we choose a 5-month lead to correspond to the onset time of the simulated biennial ENSO. Figure 6a shows the 5-month lead surface wind stress anomalies

correlated with monthly Niño3.4 SST in the control run. Only the correlation coefficients that are statistically significant (at 95% level) are highlighted in the figure. Figure 6a indicates that besides the anomalous winds in the southeast Pacific, the anomalous cross-equatorial winds in the western Pacific (west of the date line) serve as precursors of ENSO. Anomalous southeasterlies in the southern hemisphere and southwesterlies in the northern hemisphere lead matured El Niño events by two seasons. Since the simulated biennial ENSO onsets in boreal summer, it is the Indian summer monsoon and the Australian winter monsoon that matters to the onset wind pattern of the ENSO. The anomalous surface wind stress patterns associated with these two monsoon seasons in the control run are shown in Figures 6b and 6c, which were produced by correlating the two monsoon rainfall indices (i.e., AMRI and IMRI) in JJAS (June-July-August-September) with the surface wind stress anomalies in the same season. Figure 6b shows that, for a stronger-than-normal Australian winter monsoon, its anomalous wind pattern is characterized by cross-equatorial winds into the Northern Australia with northeasterlies in the northern hemisphere and northwesterlies in the southern hemisphere over the western Pacific. For a stronger-than-normal Indian summer monsoon, Figure 6c shows that a similar cross-equatorial wind pattern exists in the western Pacific, together with another northward cross-equatorial wind in the Indian Ocean converged into the Indian Peninsula. The spatial patterns of the model monsoon wind anomalies in the western Pacific resemble to and overlap very well with those associated with the onset phase of the simulated biennial ENSO.

Figure 6 suggests that the Indian and Australian monsoons simulated in CCSM3 produce surface wind stress anomalies in the western Pacific that may effectively excite the

biennial ENSO in the model, with strong (weak) Indian summer monsoon or Australian winter monsoon linked to the onset of the La Niña (El Niño) phase of the ENSO. It should be noted that the anomalous wind pattern associated with the Indian summer monsoon in the western Pacific seems to be more similar to the ENSO onset wind pattern than the Australian winter monsoon. Also as mentioned earlier, the biennial Indian monsoon variability (Figure 5b) produced in the CCSM3 control run is much stronger than the observations. The Indian summer monsoon may be more important than the Australian winter monsoon in exciting the strong biennial ENSO variability in CCSM3. However, further analyses are needed to determine their relative importance.

Besides the monsoon forcing mechanism, the warming of the equatorial Pacific mean SSTs caused by the Indian Ocean decoupling could also play a role in reducing the biennial ENSO intensity. As shown in Figure 1c, the eastern-to-central equatorial Pacific becomes warmer due to the weakening of the surface easterlies when the ocean-atmosphere coupling is turned off in the Indian Ocean. As a result, the mean east-west SST gradient along the equator is weakened. This possibly weakens the strength of the mean Pacific Walker circulation and the climatological Bjerknes feedback (Bjerknes 1969). The surface wind changes can also affect the thermocline structure along the equator. A weakening of the ocean-atmosphere coupling in the tropical Pacific may be resulted. With weaker ocean-atmosphere coupling, weaker ENSO intensity can be produced in the decoupled experiment. To examine this mechanism, we compare the coupling strengths between the control run and the decoupled experiment. Figure 7 shows the scatter plots of annual-mean surface zonal wind stress anomalies in the Niño4 (5°S-5°N,

160°E-150°W) region as a function of the SST anomalies in the Niño3.4 region for the control (blue) and decoupled (red) simulations. We select different regions for the SST and zonal wind stress anomalies to reflect their typical zonal phase shift during ENSO evolutions. The slope of the linear fit for the scattering plot, Δ(zonal wind stress anomalies)/Δ(SST anomalies), is used to estimate the coupling strength. From this figure, we find that the coupling strength for the control run is $9.6*10^{-3}$ Newton/m^2/°C but is only $0.31*10^{-3}$ Newton/m^2/°C for the decoupled experiment. This confirms our hypothesis that the warm SST bias in the tropical Indian Ocean also contributes to the strong ENSO intensity in the control run. When this warm SST bias is removed in the decoupled experiment, the Pacific surface zonal wind, and the coupling strength are reduced and lead to weaker ENSO intensity.

4. Summary and discussions

In this study, we performed two numerical experiments to examine the possible linkages between the simulated biennial ENSO and the Indian Ocean SST and Indian-Australian monsoon variability in CCSM3. We found that the excessive biennial ENSO in the model is also related to (1) the warm bias of the mean SSTs in the tropical Indian Ocean and (2) the biennial variability in Indian summer monsoon and Australian winter monsoon. The warm bias in the Indian Ocean increases the coupling strength in the tropical Pacific by inducing strong mean surface easterlies and large zonal SST gradient in the tropical Pacific, which are parts of the too strong cold tongue problem of CCSM3. We noted that the strong biennial monsoon variability in the model is capable of producing anomalous surface wind patterns in the western Pacific that

resemble the wind pattern necessary for the onset of the biennial ENSO in the model. This allows the model biennial monsoon variability to effectively excite biennial ENSO. When the warm Indian Ocean bias and the strong biennial monsoon variability are removed or weakened in an Indian Ocean-decoupled experiment, the biennial ENSO intensity is significantly reduced.

Our results suggested that besides the tropical Pacific coupling processes, the Indian Ocean and Indian-Australian monsoon variability also contribute to the excessive biennial ENSO tendency in CCSM3. Efforts that aim to alleviate the excessive biennial ENSO in CGCMs should focus not only on the processes in the tropical Pacific Ocean but also on those in the Indian Ocean and the monsoons. Our results are consistent with recent modeling studies of Watanabe (2008a, b), who demonstrated with simple and hybrid coupled models that atmosphere-ocean coupling in the Pacific can be influenced by the coupling in the Indian Ocean. As a result, the mean climate and variability of the tropical Pacific Ocean could be related to those of the tropical Indian Ocean. We should emphasize that this study adds additional possible factors to explain why the excessive biennial ENSO tendency exists in CCSM3, but does not exclude the previous explanations that emphasize the coupling processes in the Pacific Ocean. It should also be noted that the determination of the relative contribution of the Indian Ocean mean SST and monsoon variability to the biennial ENSO requires additional numerical experiments and is not addressed in this study.

Acknowledgments. The authors are grateful to Drs. Jerry Meehl, Jong-Seong Kug, and an anomalous reviewer who provide valuable comments on this paper. The authors thank Dr. Steve

Yeager of NCAR for kindly providing the restart files for the decoupled experiment. Support from NSF (ATM-0638432), NASA (NNX06AF49H), and JPL (subcontract No.1290687) are acknowledged. Model simulations and data analyses were performed at University of California, Irvine's Earth System Modeling Facility (supported by NSF ATM-0321380).

REFERENCE

Adler, R. F., et al., 2003: The version-2 global precipitation climatology project (GPCP) monthly precipitation analysis (1979-present), *J. Hydrometeorol.*, **4**(6), 1147-1167.

Chang, C.-P., and T. Li, 2000: A theory for the tropical tropospheric biennial oscillation. *J. Atmos. Sci.*, **57**, 2209-2224.

Collins, W. D., et al., 2006: The Community Climate System Model version 3 (CCSM3), *J. Clim.*, **19**(11), 2122-2143.

Deser, C., et al., 2006: Tropical pacific and Atlantic climate variability in CCSM3, *J. Clim.*, **19**(11), 2451-2481.

Hung, C. W., and M. Yanai, 2004: Factors contributing to the onset of the Australian summer monsoon, *Q. J. R. Meteorol. Soc.*, **130**(597), 739-758.

Jin, F.-F., 1997: An equatorial recharge paradigm for ENSO, I. Conceptual model. *J. Atmos. Sci.*, **54**, 811-829.

Kug, J.S., and I.S. Kang, 2006: Interactive feedback between ENSO and the Indian Ocean. *J. Clim.*, **19**, 1784–1801.

Kug J.-S., T. Li, S.-I. An, I.-S. Kang, J.-J. Luo, S. Masson, T. Yamagata, 2006: Role of the ENSO. Indian Ocean coupling on ENSO variability in a coupled GCM, *Geophys. Res. Lett.*, **33**, L09710, doi:10.1029/2005GL024916.

Li, T., P. Liu, X. Fu, B. Wang and G.A. Meehl, 2006: Tempo-spatial structures and mechanisms of the tropospheric biennial oscillation in the Indo-Pacific warm ocean regions. *J. Climate*, **19**, 3070-3087.

Loschnigg, J., G.A. Meehl, P.J. Webster, J.M. Arblaster, and G.P. Compo, 2003: The Asian monsoon, the tropospheric biennial oscillation and the Indian Ocean Dipole in the NCAR CSM. *J. Climate*, **16**, 2138-2158.

Meehl, G. A., 1987: The annual cycle and interannual variability in the tropical Pacific And Indian-Ocean regions, *Mon. Weather Rev.*, **115**, 27-50.

Meehl, G. A., 1993: A coupled air-sea biennial mechanism in the tropical Indian and Pacific regions - Role Of The Ocean, *J. Clim.*, **6**, 31-41.

Mooley, D. A., and B. Parthasarathy, 1984: Fluctuations in all-India summer monsoon rainfall during 1871-1978. *Climate Change*, **6**, 287-301.

Ogasawara, N., A. Kitoh, T. Yasunari, and A. Noda, 1999: Tropospheric biennial oscillation of the ENSO-monsoon system in the MRI coupled GCM. *J. Meteorol. Soc. Japan*, **77**, 1247-1270.

Rayner, N. A., et al., 2003: Global analyses of sea surface temperature, sea ice, and night marine air temperature since the late nineteenth century, *J. Geophys. Res.-Atmos.*, **108**,4407, doi:10.1029/2002JD002670.

Terray, P. and S. Dominiak, 2005: Indian Ocean sea surface temperature and El Nino-Southern Oscillation: A new perspective. *J. Climate*, **18**,1351-1368.

Watanabe, M., 2008a: Two regimes of the equatorial warm pool. Part I: A simple tropical climate model. *J. Climate*, **21**, 3533–3544.

Watanabe, M., 2008b: Two regimes of the equatorial warm pool. Part II: Hybrid coupled GCM experiments. *J. Climate*, **21**, 3545–3560.

Webster, P. J., C. Clark, G. Cherikova, J. Fasullo, W. Han, J. Loschnigg and K. Sahami, 2001: The monsoon as a self-regulating coupled ocean-atmosphere system. In Bob Pierce (Ed.): *Meteorology at the Millennium*, Academic Press. 650 pp.

Wyrtki, K., 1975: El Nino - The dynamic response of the equatorial Pacific Ocean to atmospheric forcing. *J. Phys. Oceanogr*., **5**, 572-584.

Wu, R. G., and B. P. Kirtman, 2004: Impacts of the Indian Ocean on the Indian summer monsoon-ENSO relationship, *J. Clim.*, **17**, 3037-3054.

Yasunari, T., 1990: Impact of Indian monsoon on the coupled atmosphere ocean system in the tropical Pacific. *Meteor. Atmos. Phys*., **44**, 29-41.

Yu, J. Y., et al., 2002: Impacts of the Indian Ocean on the ENSO cycle, *Geophys. Res. Lett.*, **29**, 1204, doi:10.1029/2001GL014098.

Yu, J. Y., et al., 2003: Ocean roles in the TBO transitions of the Indian-Australian monsoon system, *J. Clim.*, **16**, 3072-3080.

FIGURE CAPTIONS

Figure 1. Long-term mean SSTs from (a) the HadISST and (b) the CCSM3 control run. Panel (c) shows the SST differences between the decoupled experiment and the control run. Contour intervals are 1°C for (a) and (b) and 0.5°C for (c). Positive values in (c) and values greater than 28°C in (a) and (b) are shaded. Negative values in (c) are dashed.

Figure 2. Standard deviations of interannual SST anomalies calculated from (a) the CCSM3 control run and (b) the Indian Ocean decoupled experiment. Contour intervals are 0.2°C.

Figure 3. Seasonal variations of the standard deviations of Niño3.4 SST anomalies calculated from the CCSM3 control run (solid) and the Indian Ocean decoupled experiment (dashed). The abscissa is the calendar month and the ordinate shows the standard deviations in degree C.

Figure 4. Power spectra of monthly Niño3.4 SST anomalies from the CCSM3 control run (blue) and the Indian Ocean decoupled experiment (red). Dashed curves are the AR1 red noise at 95% significant level.

Figure 5. Power spectra of monthly (a) AMRI and (b) IMRI from the observations (GPCP, black), the CCSM3 control run (blue), and the Indian Ocean decoupled experiment (red). Dashed curves are the AR1 red noise at 95% significant level.

Figure 6. Simulated correlation coefficients between (a) 5-month lead surface wind stress anomalies with monthly Niño3.4 SST anomalies; (b) JJAS surface wind stress anomalies with JJAS AMRI; (c) JJAS surface wind stress anomalies with JJAS IMRI for the CCSM3 control run. Only correlation coefficients above 95% significant level are highlighted.

Figure 7. Scatter plots of annual mean surface zonal wind stress anomalies averaged over Niño4 region and SST anomalies averaged over the Niño3.4 region from the CCSM3 control run (blue) and the Indian Ocean decoupled experiment (red). The linear regression fits are also shown.

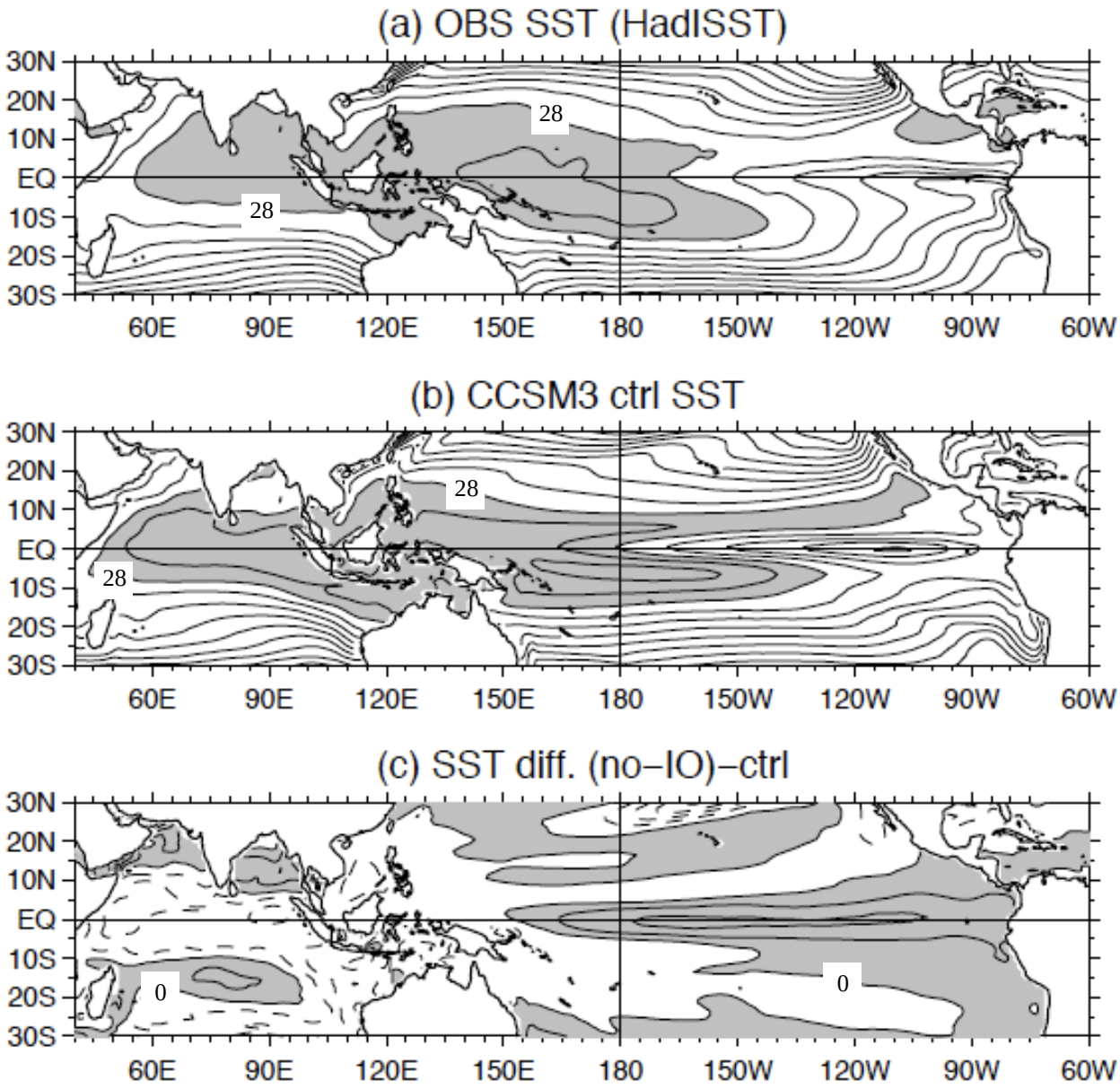

Figure 1. Long-term mean SSTs from (a) the HadISST and (b) the CCSM3 control run. Panel (c) shows the SST differences between the decoupled experiment and the control run. Contour intervals are 1°C for (a) and (b) and 0.5°C for (c). Positive values in (c) and values greater than 28°C in (a) and (b) are shaded. Negative values in (c) are dashed.

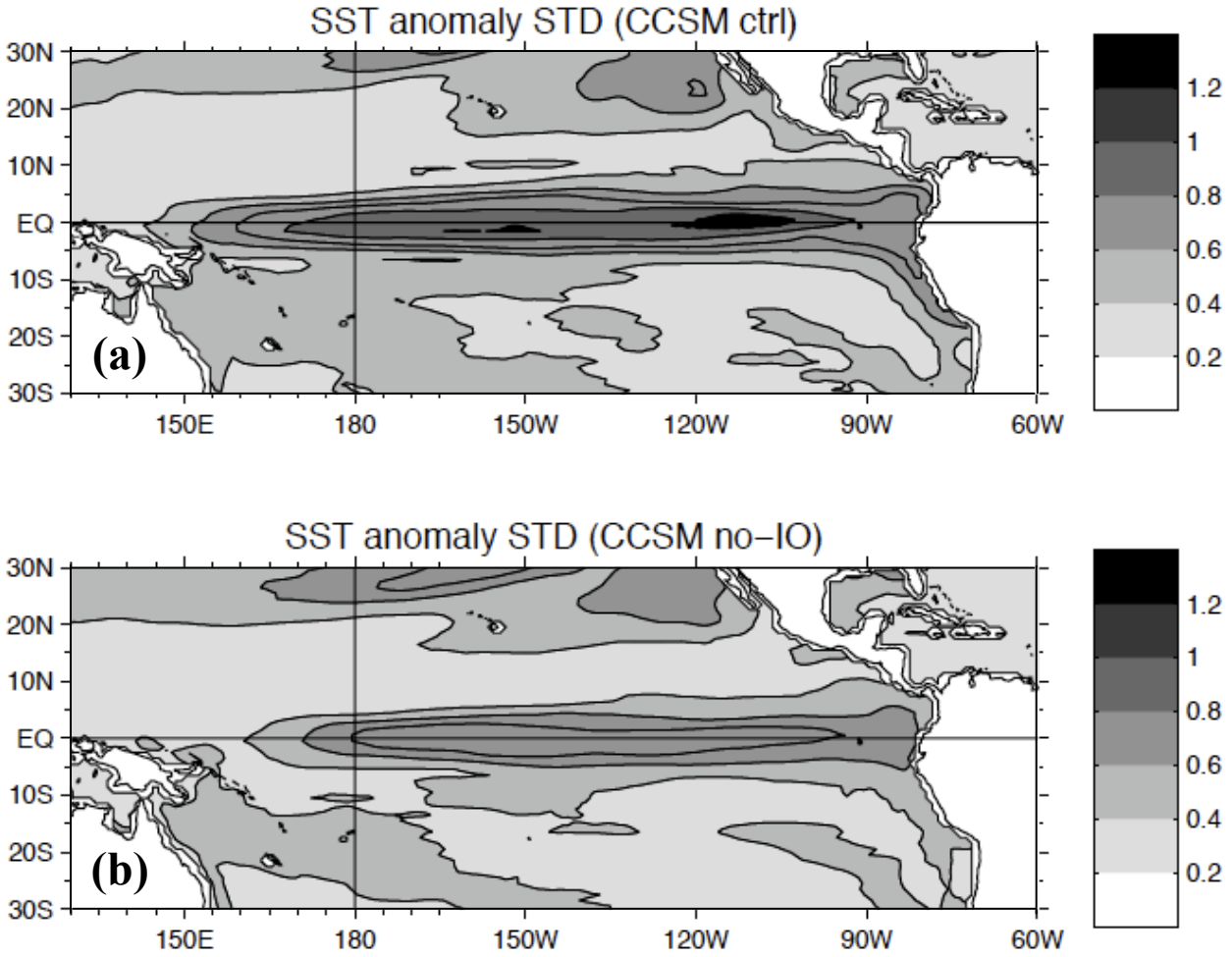

Figure 2. Standard deviations of interannual SST anomalies calculated from (a) the CCSM3 control run and (b) the Indian Ocean decoupled experiment. Contour intervals are 0.2°C.

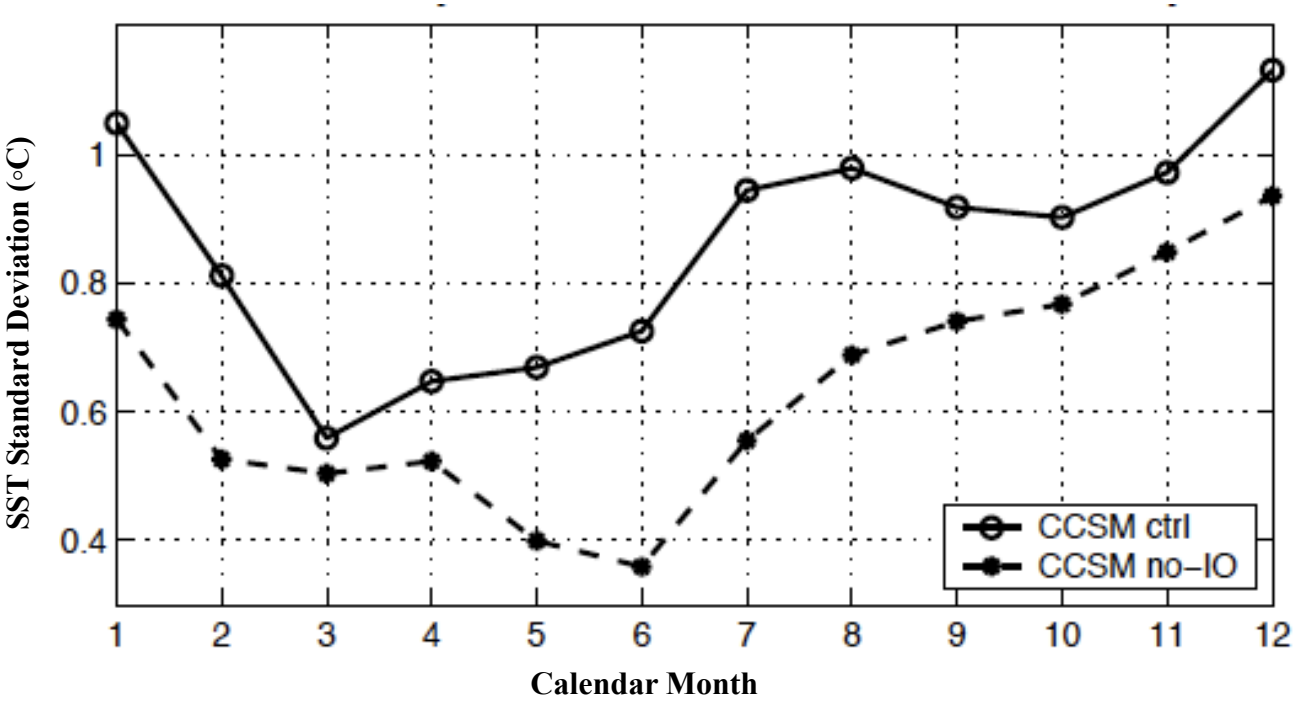

Figure 3. Seasonal variations of the standard deviations of Niño3.4 SST anomalies calculated from the CCSM3 control run (solid) and the Indian Ocean decoupled experiment (dashed). The abscissa is the calendar month and the ordinate shows the standard deviations in degree C.

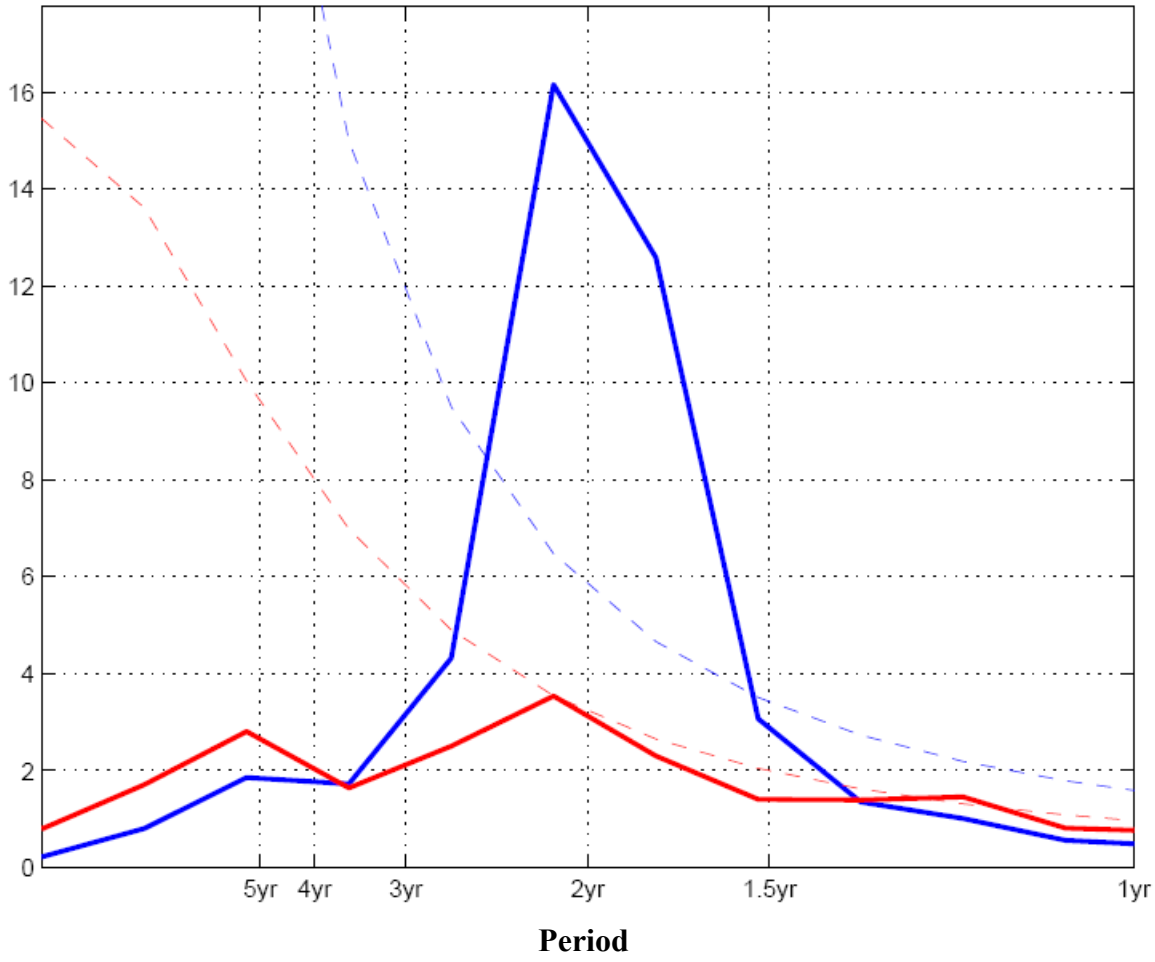

Figure 4. Power spectra of monthly Niño3.4 SST anomalies from the CCSM3 control run (blue) and the Indian Ocean decoupled experiment (red). Dashed curves are the AR1 red noise at 95% significant level.

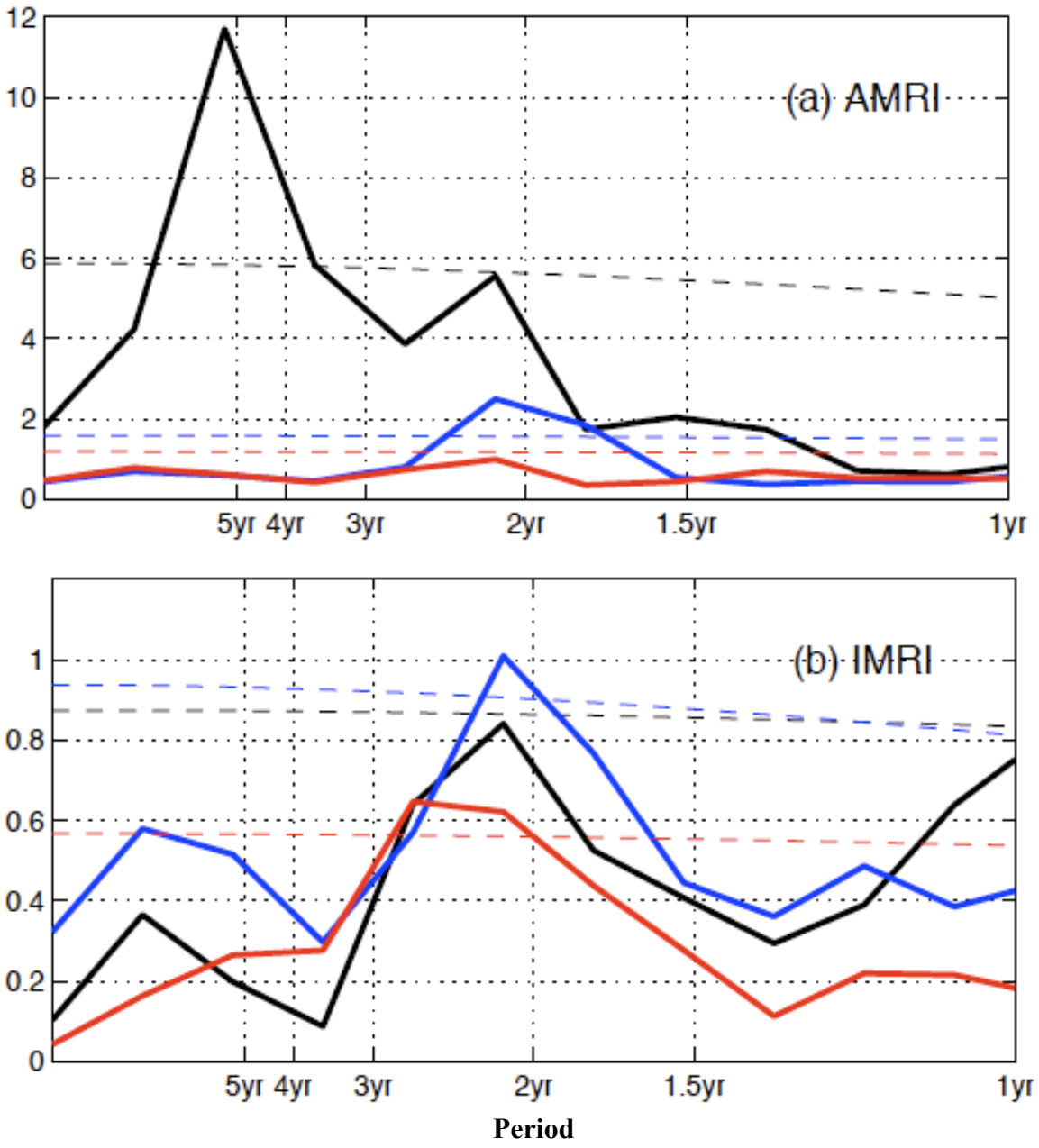

Figure 5. Power spectra of monthly (a) AMRI and (b) IMRI from the observations (GPCP, black), the CCSM3 control run (blue), and the Indian Ocean decoupled experiment (red). Dashed curves are the AR1 red noise at 95% significant level.

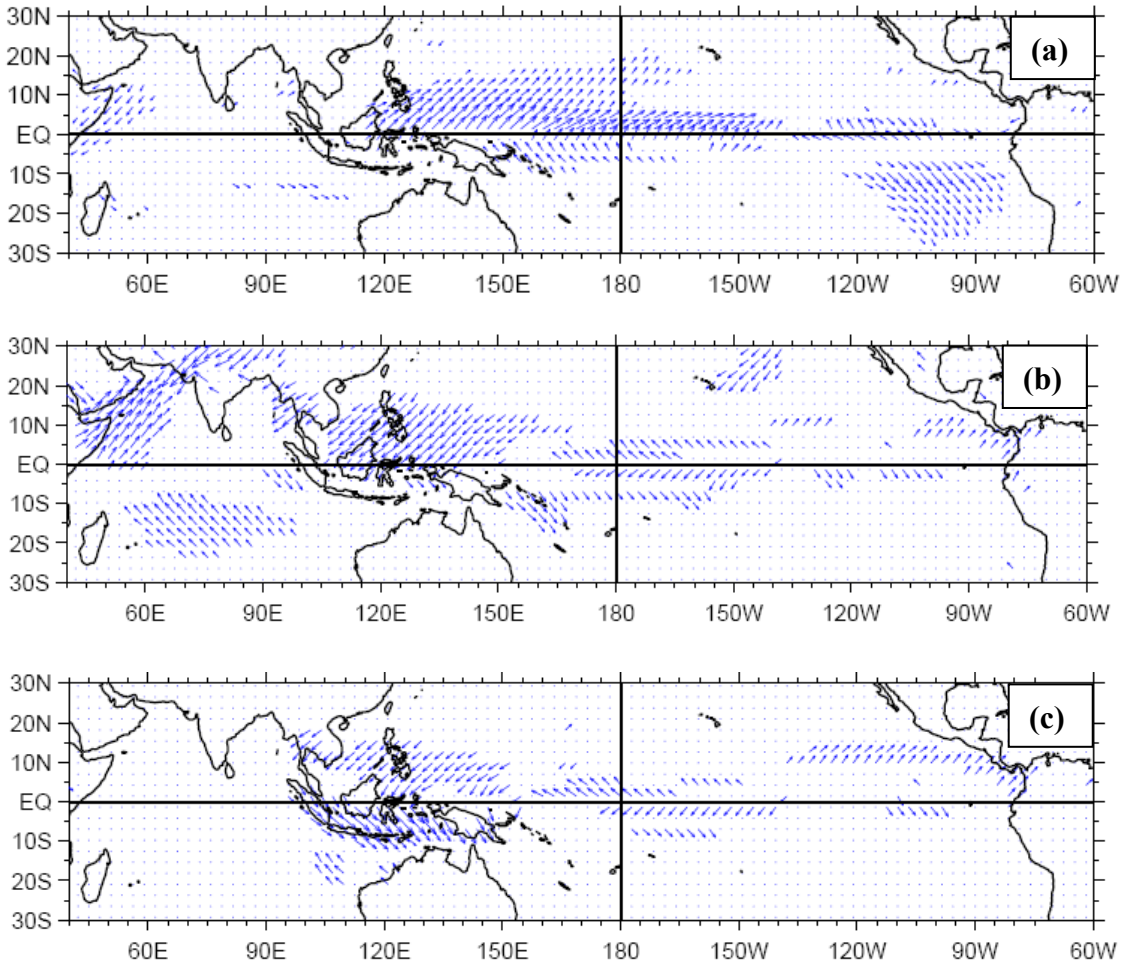

Figure 6. Simulated correlation coefficients between (a) 5-month lead surface wind stress anomalies with monthly Niño3.4 SST anomalies; (b) JJAS surface wind stress anomalies with JJAS AMRI; (c) JJAS surface wind stress anomalies with JJAS IMRI for the CCSM3 control run. Only correlation coefficients above 95% significant level are highlighted.

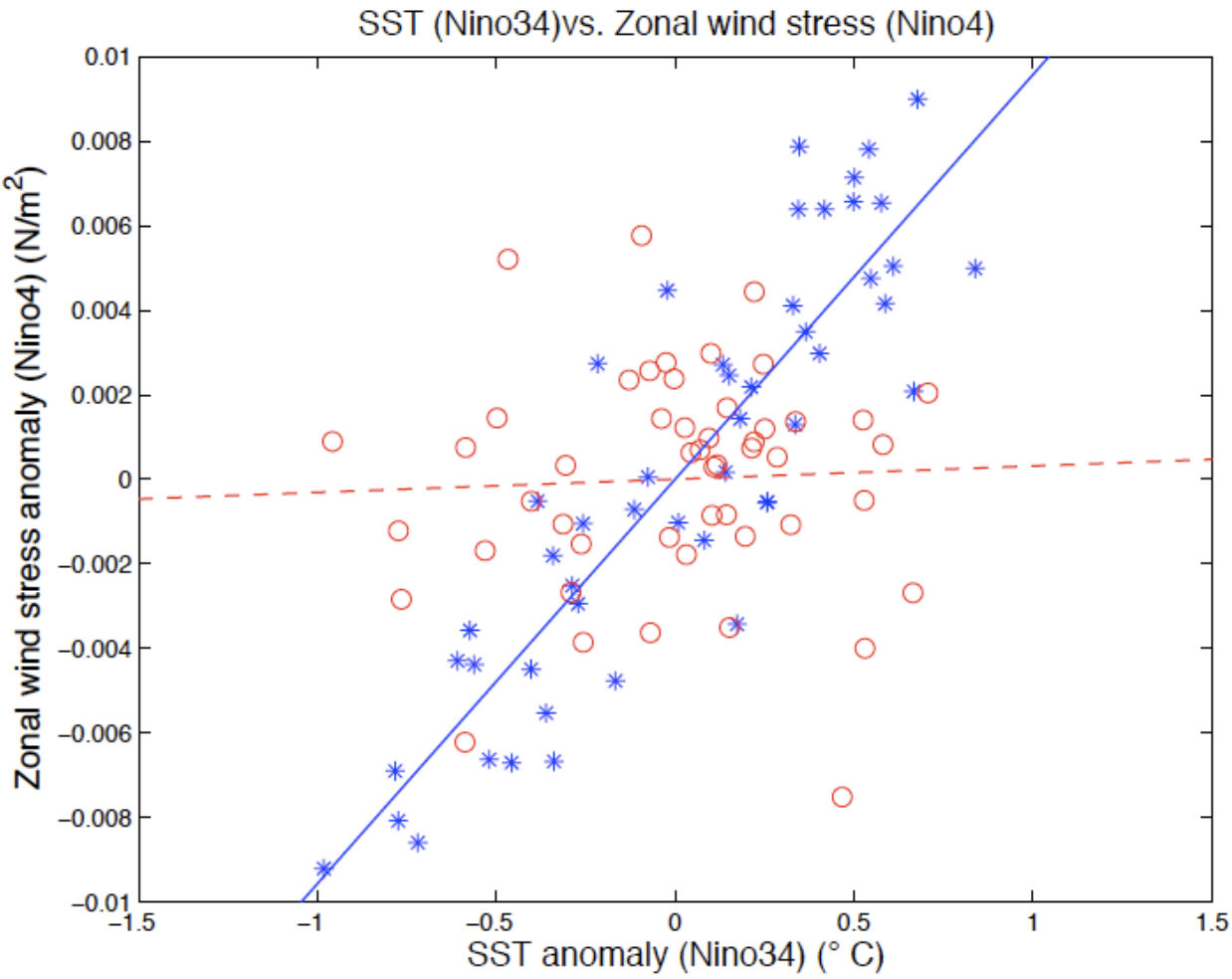

Figure 7. Scatter plots of annual mean surface zonal wind stress anomalies averaged over Niño4 region and SST anomalies averaged over the Niño3.4 region from the CCSM3 control run (blue) and the Indian Ocean decoupled experiment (red). The linear regression fits are also shown.